PERIODICO di MINERALOGIA
established in 1930

DIPARTIMENTO DI SCIENZE DELLA TERRA
SAPIENZA UNIVERSITÀ DI ROMA

An International Journal of
Mineralogy, Crystallography, Geochemistry,
Ore Deposits, Petrology, Volcanology
and applied topics on Environment, Archaeometry and Cultural Heritage

Mineral chemistry and geothermobarometry of adakitic rocks from Kashan, central Urumieh-Dokhtar magmatic arc, Iran: implications for magma evolution

Tayebeh Khaksar [1,*], Ali Reza Davoudian [1], Sakine Moradi [2], Nahid Shabanian [1], Shu -Guang Song [3]

Faculty of Natural Resources and Earth Sciences, Shahrekord University, Shahrekord, Iran
State Key Laboratory of Critical Mineral Research and Exploration, Institute of Geochemistry, Chinese Academy of Sciences, Guiyang 550081, China
Department of Geology, School of Earth and Space Sciences, Peking University, Beijing, China

ARTICLE INFO

Submitted: December 2024
Accepted: April 2025
Available on line: April 2025

* Corresponding author:
Khaksar.tayebe3631@gmail.com

Doi: 10.13133/2239-1002/18746

How to cite this article:
Khaksar T. et al. (2025)
Period. Mineral. 94, 67-82

ABSTRACT

The Kashan region is located in the central part of the Urumieh-Dokhtar magmatic Arc (UDMA). In this area, Miocene adakitic rocks, including andesites and rhyodacites, occur as lava flows and domes. The primary mineral assemblages consist of amphibole, biotite and plagioclase, with minor alkali feldspar. Mineral chemistry analyses reveal that plagioclase compositions from andesine to oligoclase, amphiboles vary from Mg-hastingsite, tschermakite to Mg-hornblende, and biotites span from annite to phlogopite. Amphiboles show high $Fe^{3+}/(Fe^{3+}+Fe^{2+})$ ratios, whereas magmatic biotites in rhyodacites exhibit low total Al and narrow Fe/(Fe+Mg) ratios, indicative of relatively oxidizing conditions. Oxygen fugacity (fO_2) values range from $10^{-10.4}$ bar (ΔNNO+0.75, representing nickel-nickel oxide) in andesites to $10^{-12.3}$ bar (ΔNNO+1.7) in rhyodacites. Application of the calcic amphibole geothermobarometer indicates that amphiboles crystallized at temperatures of 791-986 °C and pressures of 620-800 MPa in andesites, and at 636-850 °C and 250-450 MPa in rhyodacitic rocks, corresponding to maximum crustal depths of 28 km. Primary biotites in rhyodacites crystallized slightly later at temperatures of 690-784 °C (average 712 °C).

Keywords: Mineral chemistry; geothermobarometry; adakite; Urumieh-Dokhtar magmatic arc; Iran.

INTRODUCTION

Geothermobarometric techniques play a crucial role in better assessment of the tectonic processes that shape the geological evolution of specific regions (e.g., Szymanowski et al., 2017; Fanka et al., 2018). These techniques are based on the chemical potential of elements in rock-forming minerals, which are influenced by the chemistry of the melt and the evolving thermodynamic conditions during crystallization (e.g., Abbott and Clarke, 1979; Helmy et al., 2004). As a result, the mineralogical characteristics of rocks provide valuable insights into the physicochemical conditions, such as temperature, pressure and oxygen fugacity, that prevailed during their formations (Helmy et al., 2004). Accurate pressure and temperature estimations are crucial for interpreting geological evolution, and are typically integrated with field observations, petrographic analyses, geochemical data, structural studies, and geochronological investigations.

Amphiboles are key minerals in a wide range of igneous and metamorphic rocks. Thermobarometric of amphibole and clinopyroxene are commonly used to determine the pressure- temperature (P-T) conditions during the

emplacement of igneous rocks, providing insight into the depth of their intrusion (e.g., Putirka, 2008b; Ridolfi et al., 2010). Variations in the aluminum (Al) content of calcic amphiboles, for instance, are closely associated with the depth of pluton emplacement. Over the last three decades, Al-in-hornblende geobarometry has been widely applied to determine the emplacement depths of plutons (e.g., Rutter et al., 1989; Anderson, 1996; Anderson et al., 2008; Hossain et al., 2009). Such information is crucial for understanding the spatial, temporal, and chemical evolution of the orogenic systems (Rutter et al., 1989). Biotite is another important ferromagnesian mineral, commonly found in intermediate and felsic rocks. Its composition is primarily influenced by magma characteristics and the physicochemical conditions during crystallization (e.g., Abdel-Rahman, 1994).

The Kashan adakitic rocks, comprising andesites and rhyodacites, are characterized by major minerals such as amphibole, plagioclase, and biotite. This study utilizes mineral chemistry, with a focus on amphibole and biotite compositions, to investigate the geological conditions that influenced the formation of Miocene adakitic rocks in the southern Kashan region. We have used mineral compositions to evaluate the pressure-temperature (P-T) conditions, the magmatic series, and the evolution of the magmas that formed these rocks, as well as to investigate the depth of the associated magma chambers.

GEOLOGICAL BACKGROUND

The Zagros orogen, a segment of the Alpine-Himalayan orogenic system, formed by the closure of the Neo-Tethyan oceanic basement subsequent continental collision between the Arabian and Iranian blocks during Cenozoic (e.g., Mohajjel and Fergusson, 2000; Agard et al., 2005). Structurally, the Zagros orogen is divided into three principal segments (e.g., Mohajjel et al., 2003; Alavi, 2004): the Zagros Fold-Thrust Belt (ZFTB; e.g., Berberian and King, 1981), the Sanandaj-Sirjan Zone (SaSZ; e.g., Stocklin, 1968), and the Urumieh-Dokhtar Magmatic Arc (UDMA; e.g., McClusky et al., 2003) (Figure 1a). The ZFTB and the SaSZ consist of folded and faulted sequences: the ZFTB contains Paleozoic-Mesozoic shelf deposits, whereas the SaSZ includes significantly Precambrian- Paleozoic metamorphic rocks (e.g., Stocklin, 1968; Davoudian et al., 2022) resulting from continental intra-subduction before Neo-Tethyan subduction (Shabanian and Neubauer, 2024).

The UDMA originated from the subduction of the Neo-Tethyan oceanic slab, followed by the collision of the Arabia and Eurasia continents, likely occurring from the Late Cretaceous to the Pliocene (e.g., Berberian and King, 1981; Agard et al., 2011; Chiu et al., 2013). Magmatic activity in the UDMA decreased from the Late Miocene to the Quaternary compared to the Paleogene. However, during this time, various magma types erupted, including ultrapotassic (Ahmadzadeh et al., 2010; Pang et al., 2013b), adakitic (e.g., Jahangiri, 2007; Khodami et al., 2009), alkali basaltic magmas (e.g., Pang et al., 2012; Allen et al., 2013), high-K calc-alkaline and shoshonitic magmas (e.g., Khaksar et al., 2020, 2022; Moradi et al., 2022; Dargahi et al., 2007). Several models have been proposed to explain adakitic magmatism in continental collision zones, including: (1) partial melting of a detached oceanic slab (e.g., Omrani et al., 2008), (2) in-situ melting of the thickened lower crust (e.g. Pang et al., 2016), (3) magmatic reprocessing of subducted or delaminated lower crust (e.g., Karsli et al., 2010), and (4) garnet and/or amphibole fractionation affecting mantle wedge-derived magmas (e.g., Song et al., 2014). Adakitic rocks in the UDMA have been extensively studied across a broad geographical area, ranging from the northern (e.g., Azizi et al., 2024) to the central (Chiu et al., 2013; Ghorbani et al., 2014; Pang et al., 2016) and extending to the southern regions (e.g., Kheirkhah et al., 2020). The timing of adakites formation in Iran varies significantly, from Paleozoic in Central Iran (Torabi, 2012; Delavari et al., 2014) to Pleistocene in the southern UDMA (Pang et al., 2016). Most adakites in Iran are attributed to oceanic slab melting (e.g., Jahangiri, 2007; Khodami et al., 2009), or partial melting of the lower crust (e.g., Pang et al., 2016; Azizi et al., 2024), in a post-collisional setting.

The Middle Miocene Kashan volcanic rocks are located in southern Kashan in Central UDMA (Chiu et al., 2013). They are composed of andesite and rhyodacite which are characterized by adakitic geochemical affinities (Khaksar et al, unpubl. data). Samples were collected from five volcanic cones near the cities of Kamo, Choghan, Azran, Joshaghan, and Kuh-e-Chehle-Dokhtaran (Figure 1b). Field observations indicate that the exposed lithology in the area could be summarized as follows: (1) Early to Late Eocene effusive green tuff and pyroclastic rocks, (2) Oligocene sedimentary rocks (Lower Red Formation), and (3) Early to Middle Miocene volcanic rocks (as documented here). The Kashan adakitic rocks are predominantly found as small dome-shaped bodies with light to dark gray, and exhibit a porphyritic texture. These rocks commonly intrude Eocene pyroclastic units (Figure 2a) and occasionally intersect Early Miocene south Kashan granitoid as domes (Figure 2b) or dykes (Figure 2c). Moreover, they exhibit characteristic columnar-jointed structures at some locations (Figure 2d).

ANALYTICAL METHOD

Eleven samples of rhyodacitic and andesitic rocks were selected for mineral phase analysis. Thin sections were prepared and polished for mineralogical examination.

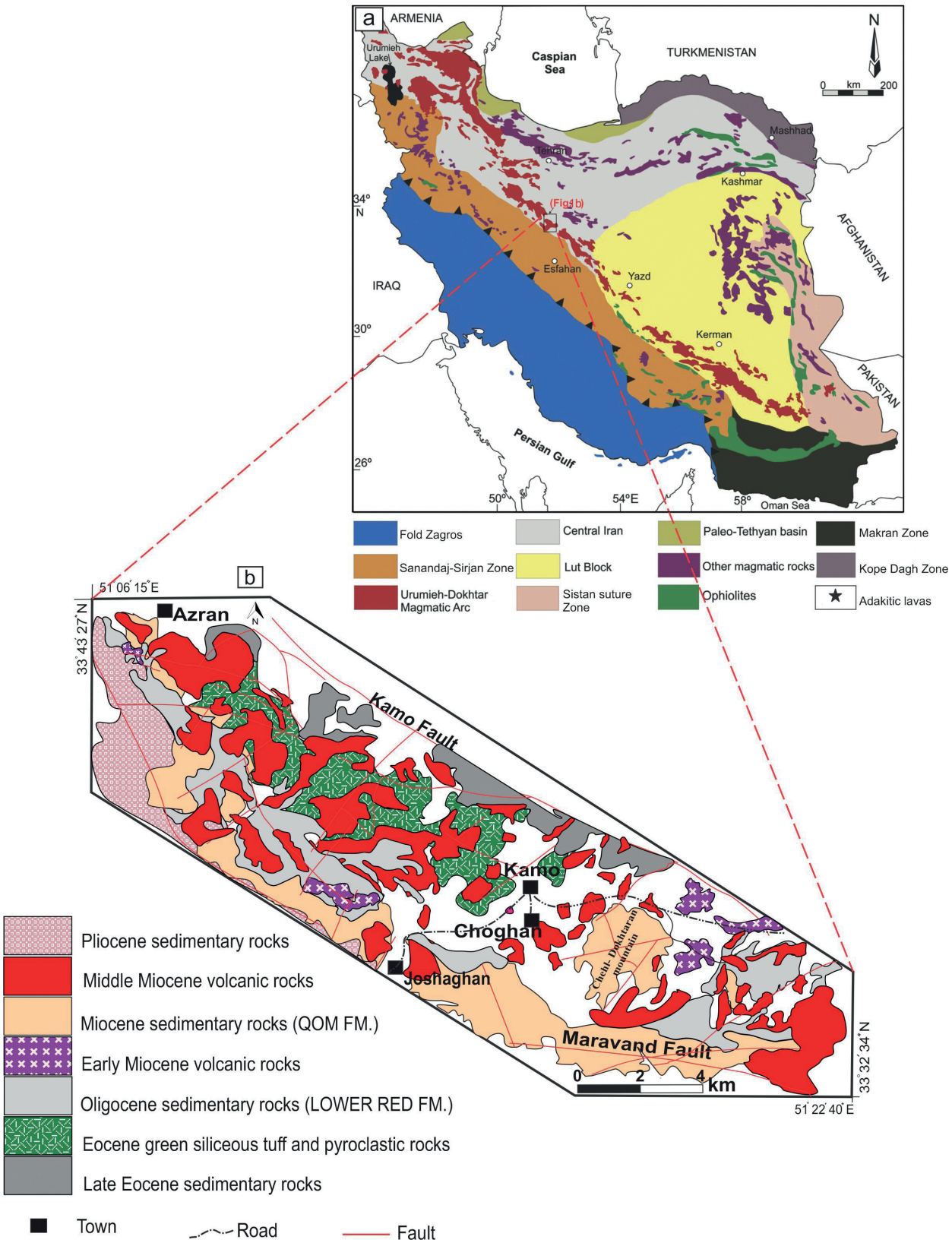

Figure 1. a) A simplified overview map of Iran showing the main structural units (modified after Stocklin, 1968) and the location of the study area; b) Simplified geological map of the region (modified after Radfar, 1993). (Abbreviation: Fm= Formation).

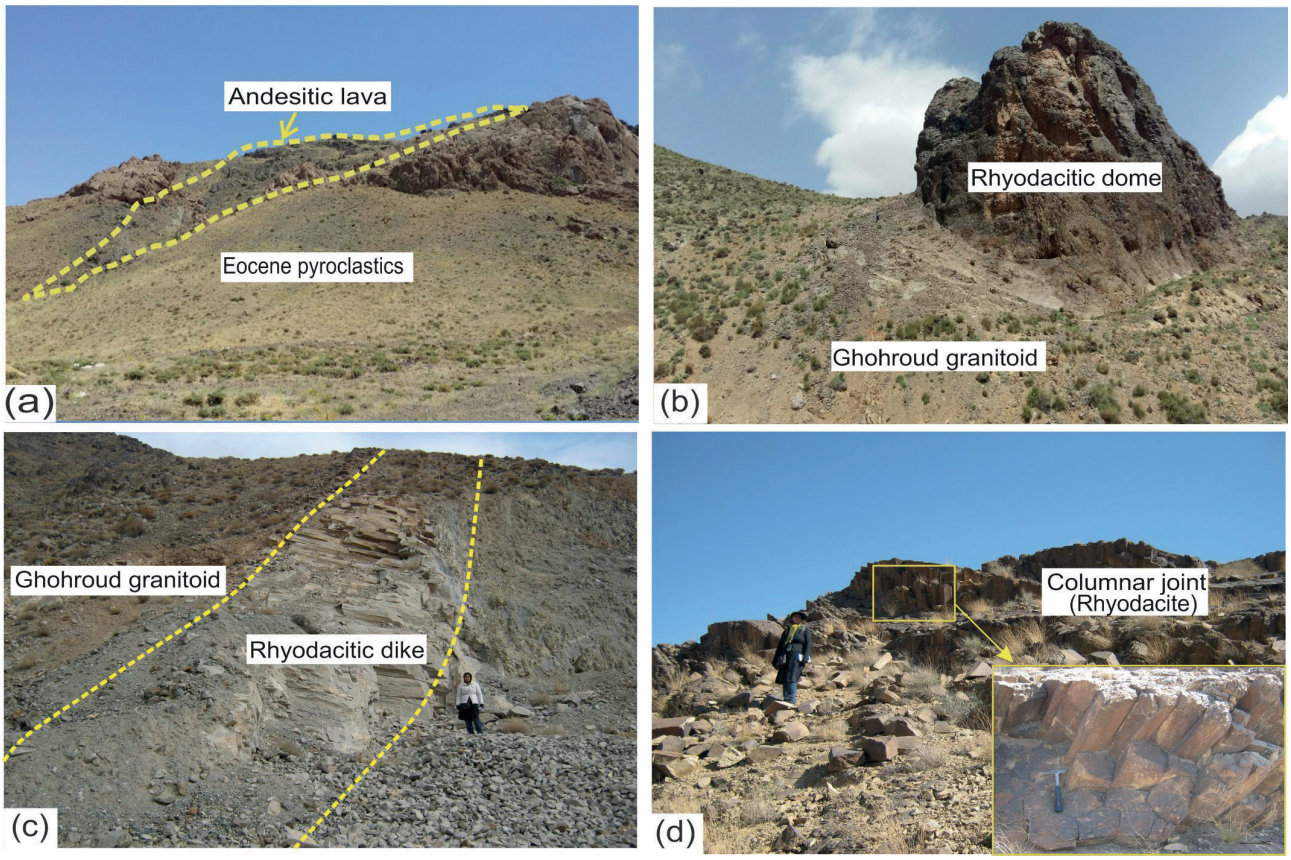

Figure 2. a) Field images from Kashan adakitic rocks. (a) The sharp contact between andesitic lava and Eocene pyroclastic units; (b) outcrops of a rhytodacitic dome and (c) a dyke, both cutting the Early Miocene Ghohroud granitoid; (d) columnar-jointed structures in rhyodacite in the northern sector of the study area.

Representative samples were analyzed using an electron probe micro-analyzer (EPMA) (JEOL JXA-8100), at Peking University, operated at an acceleration voltage of 15 kV, with a beam current of 20 nA and a beam spot size of 1-5 μm. Routine analyses were involved counting for 20 s at the peak and 5 s in the background. Standards for this analyses included synthetic silica for Si and synthetic spessartine for Mn, and natural minerals including such as sanidine for K, pyrope for Mg, andradite for Fe and Ca, albite for Na and Al, and rutile for Ti. K-alpha emissions were acquired for all elements except Ba, for which the L-alpha emission was used. Ferric iron content in the minerals was determined using the methodology described by Droop (1987).

RESULTS

Petrography

The andesitic rocks exhibit a porphyritic texture comprise of plagioclase (~50-60 vol%) and amphibole (~20-30 vol%) phenocrysts as primary minerals, along with plagioclase, biotite (~5-10 vol%), and Fe-Ti oxide (~3-5 vol%) in the matrix (Figure 3a). Amphibole, plagioclase, and opaque minerals in these rocks occasionally display a glomeroporphyritic texture (Figure 3a). Plagioclase phenocrysts (0.5-3 mm) are subhedral to euhedral and some of them exhibit sieve textures and oscillatory zoning (Figure 3b). Plagioclase phenocrysts show partial replacement by secondary minerals such as sericite and chlorite rarely.

Elongated prismatic hornblende phenocrysts are euhedral to subhedral, with smaller, lath-shaped grains, which some of them enclose fine-grained minerals such as plagioclase with twinning texture and minor opaque, (Figure 3 a,b). Locally, amphibole grains have undergone alteration to chlorite, epidote, actinolite, and titanite, particularly along the rims. Accessory minerals present in these rocks include apatite, Fe-Ti oxides, and rare alkali feldspar.

The rhyodacitic rocks exhibit porphyritic textures, characterized by quartz (20-25 vol%), alkali-feldspar (4-17 vol%), plagioclase (8-14 vol%), biotite (~10 vol%) and rare amphibole phenocrysts within a microcrystalline groundmass composed primarily of quartz, sodic

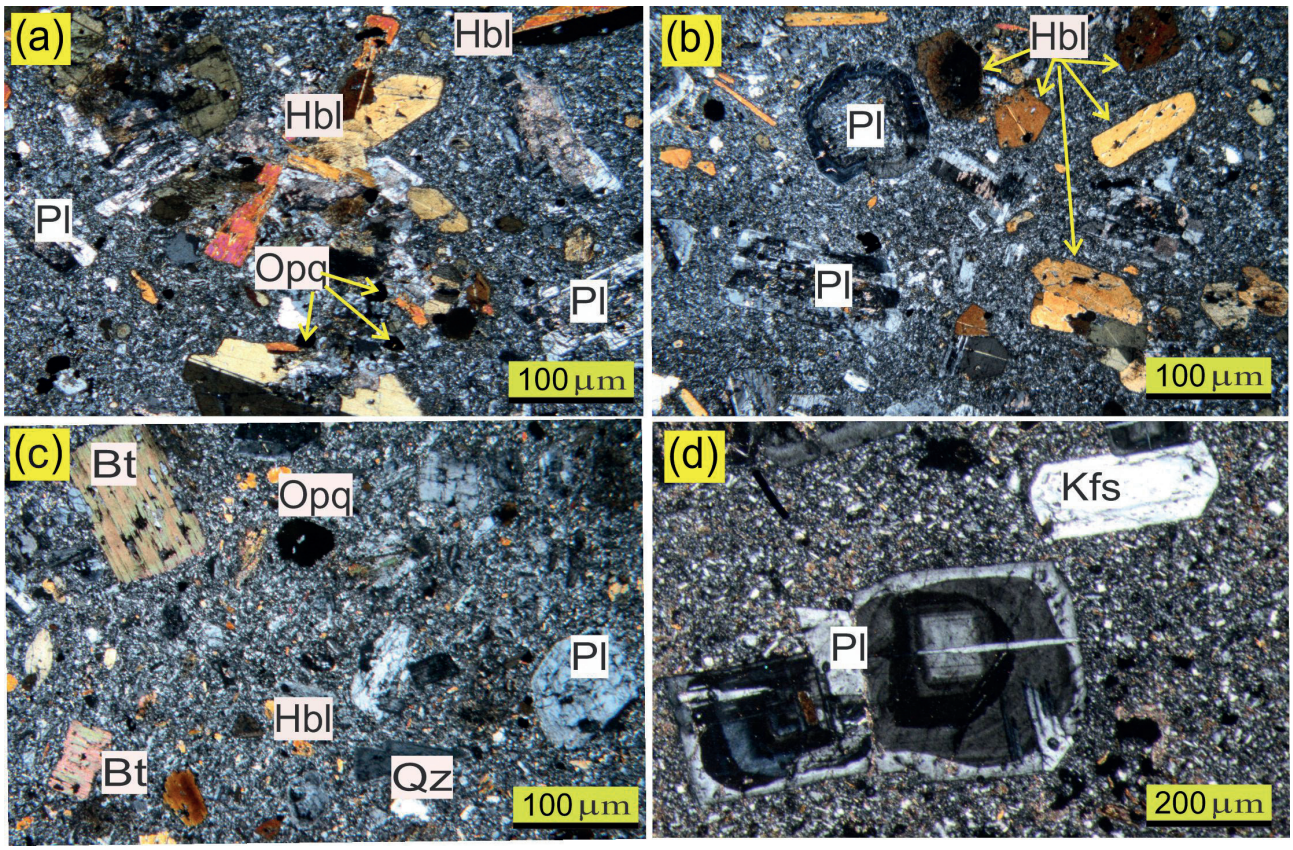

Figure 3. Micro-photomicrographs of the Kashan adakites. (a-b) Porphyritic texture of the andesite with hornblende and plagioclase phenocrysts (cross-polarized light); (c-d) plagioclase, K-feldspar and biotite phenocrysts in a groundmass of feldspar, biotite and hornblende in the rhyodacite (cross-polarized light). Mineral abbreviations: Pl. Plagioclase; Hbl. Hornblende; Bt. Biotite; Kfs. K-feldspar; Qz. Quartz; Opq. Opaque, (Whitney and Evans, 2010).

plagioclase and alkali-feldspar. They commonly undergo alteration to epidote and calcite, whereas K-feldspars phenocrysts altered to sericite. Feldspar phenocrysts are typically euhedral, although some display partial resorption and sieved textures (Figure 3c). Some plagioclase exhibits not only oscillatory zoning but also normal and reversed zoning (Figure 3d). Biotite occurs as brown flakes, sometimes replaced by chlorite along their rims. Accessory phases include titanite, zircon, apatite, and Fe-oxide.

Petrographic evidence indicates the following crystallization sequence: amphibole and plagioclase → plagioclase → biotite and Fe-Ti oxides → accessory minerals. The main petrographic characteristics of the samples are summarized in Table 1.

Table 1. Summarized petrographic characteristics of Kashan rocks in this study.

Rock type	Texture	Main minerals	Accessory minerals	Modal (%)
Andesite	Porphyry, Glomeroporphyry	Plagioclase, amphibole, biotite	Apatite, Fe-Ti oxides, alkali feldspar	Plagioclase (50-60 vol%), Amphibole (20-30 vol%), Biotite (5-10 vol%), Fe-Ti oxides (3-5 vol%), Accessory minerals (<3 vol%)
Rhyodacite	Porphyry	Plagioclase, quartz , K-feldspar, biotite	Titanite, zircon, apatite, Fe-oxide	Quartz (20-25 vol%), Alkali-feldspar (4-17 vol%), Plagioclase (8-14 vol%), Biotite (~10 vol%)

Mineral chemistry

Feldspars

The chemical compositions of the representative feldspar phenocrysts are presented in Table S1. Plagioclase, occurring phenocrysts, microcrysts, and microlites are the predominant rock-forming mineral in the studied rocks. Based on the Ab-An-Or ternary diagram developed by Deer et al. (1966) (Figure 4), plagioclases in the andesitic samples is classified as andesine (An_{36-43}), along with K-feldspars with a composition of Or_{93-95}. In the rhyodacitic samples, plagioclase predominantly plots in the andesine (An_{36-43}) to oligoclase ($An3_{6-43}$) fields. K-feldspar composition in these rocks is Or_{88-91}. As a result, plagioclase compositions predominantly fall within the oligoclase to andesine range in the studied rock. The normal, reverse, and oscillatory zoning observed in plagioclase phenocrysts are closely associated with chemical variations within these minerals. For instance, normal zoning in plagioclase phenocrysts from andesite rocks is characterized by a decrease in An content from core to rim, whereas reverse zoning indicates an increase in An content from core to rim. These chemical variations highlight different mechanisms of magma evolution during crystallization.

Amphibole

Amphibole phenocrysts measurements were carried out on adakitic andesitic and rhyodacitic rocks. The chemical compositions of these amphiboles are presented in Table S2, with classification diagrams shown in Figure 5.

The amphiboles from the andesitic and rhyodacitic samples exhibit high CaO (9.67 wt%-11.46 wt%), high MgO (11.79 wt%-15.70 wt%), and low Na_2O (1.20 wt%-2.54 wt%), consistent with chemical characteristics of calcic amphiboles [CaB≥1.5; (Na+K)A<0.5] (Figure 5). Based on the Si versus Na+K diagram (Leak et al., 1997) the amphiboles of the rhyodacitic and andesitic rocks

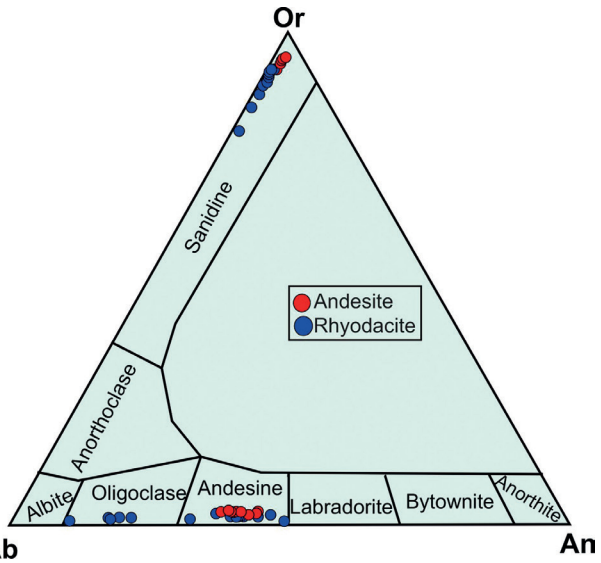

Figure 4. Ab-An-Or Classification diagram for plagioclase and K-feldspar compositions from the Kasan adakites.

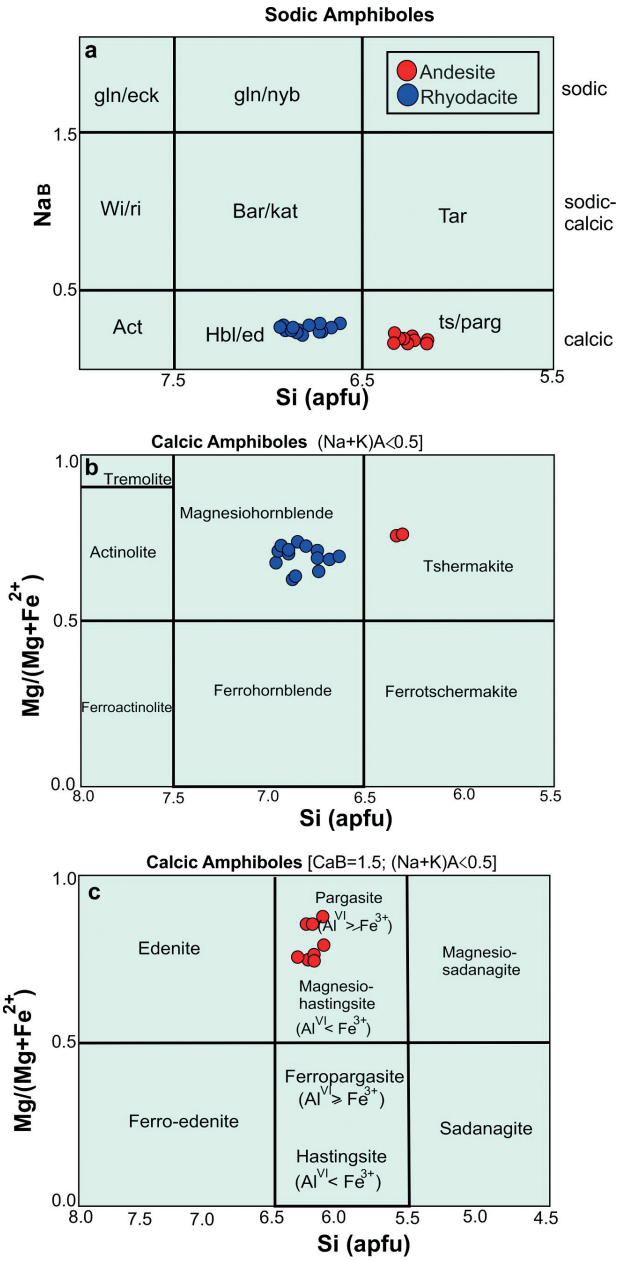

Figure 5. Classification diagrams of (a) sodic and (b,c) calcic amphiboles (Leake et al., 1997). Abbreviations: Gln=Glaucophane, Nyb=nybøite; Eck=Eckermannite; Wi/Ri=Winchite/Richterite, Bar/Kat=Barroisite/Katophorite, Tar=Taramite, Act=Actinolite; Hbl/Ed=Hornblende/Edenite, Ts/Parg=Tschermakite/Pargasite.

are classified as hornblende/edenite and tschermakite/pargasite, respectively (Figure 5a). In the Mg/(Mg+Fe^{2+}) versus Si diagrams, amphiboles in rhyodacitic rocks exhibit Mg-hornblende composition (Figure 5b). According to the values of Al^{VI} and Fe^{3+} cations per formula unit, amphiboles in andesitic samples range from tschermakite/pargasite to magnesian-hastingsite, as illustrated in Figure 5c.

Mica

The brown mica content in the both andesitic and rhyodacitic rocks are significantly lower than that of amphibole. The chemical compositions of these minerals are summarized in Table S3. In the classification diagram presented by Leake et al. (1997), which categorizes micas based on the Mg/(Mg+Fe^{2+}) ratio and Al^{IV} -1 contents, all samples are located within the biotite range, although some micas in the rhyodacitic samples straddle the biotite and phlogopite fields (Figure 6a). In the biotite classification diagram (Figure 6b), biotite from the andesitic samples categorized as Fe-biotite, while the biotite from the rhyodacite samples is identified as Mg-biotite. Figure 6c (10 TiO_2-FeO-MgO diagram) shows the biotite compositions plotted on the Nachit et al. (2005) diagram, which is primarily used for intrusive rocks to distinguish primary, re-equilibrated, and neoformed biotites. In this study, we apply it to volcanic samples to assess potential hydrothermal alteration. The results indicate that biotites from rhyodacitic samples fall within the primary biotite field, whereas those from andesites plot in the re-equilibration field, suggesting possible post-magmatic modification. The composition of biotite varies depending on the granite type such as Al-rich in peraluminous (S-type) granites, Mg-rich in calc-alkaline

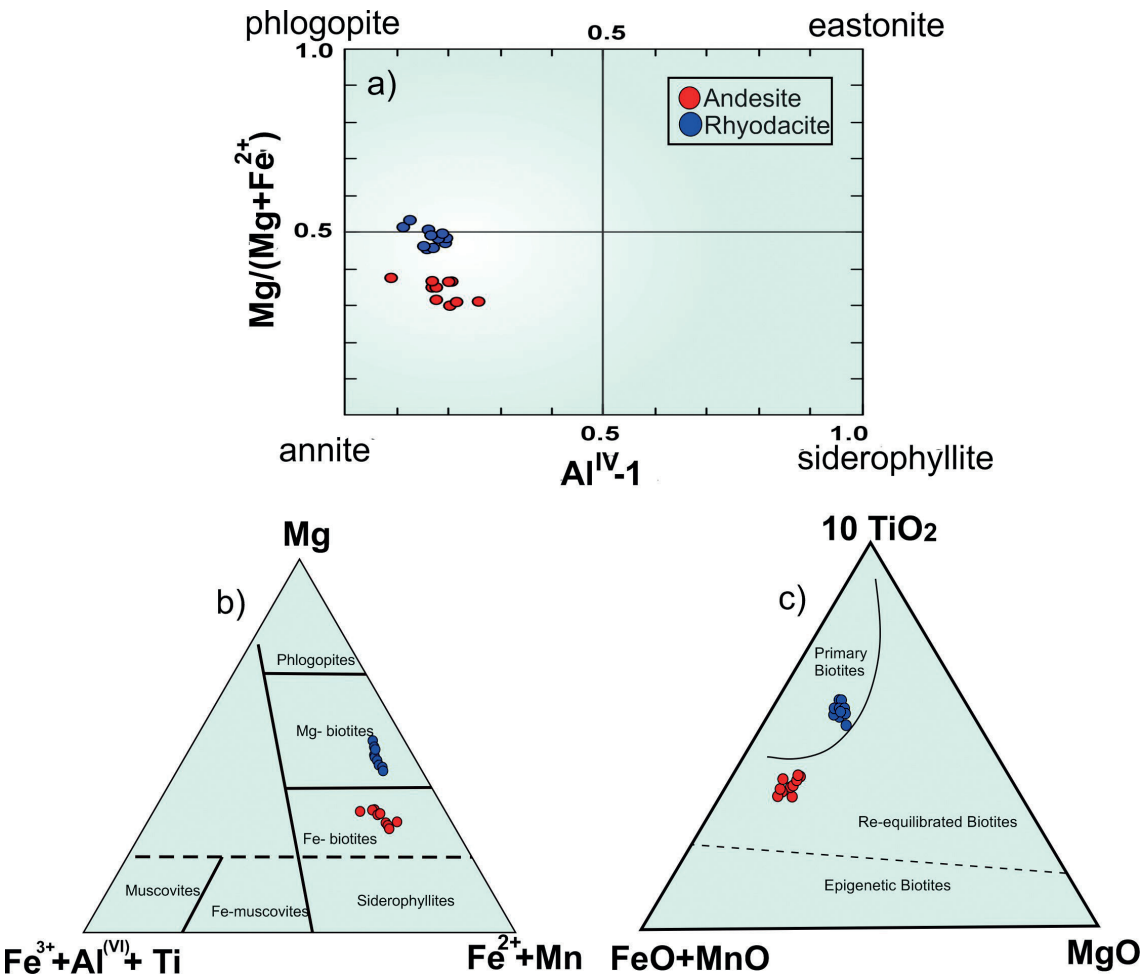

Figure 6. a) Mg/(Mg+Fe^{2+}) versus Al IV-1 classification diagram for biotites (Leake et al., 1997); b) 10.TiO_2-FeO*-MgO ternary discrimination diagram of primary, re-equilibrated, and epigenetic biotite (Nachit et al. 2005); c) Ternary Mg–(Fe^{2+}+Mn)-(Al^{VI}+Fe^{3+}+Ti) classification diagram of biotite (Foster, 1960). (Elements are in atom per formula unit (a.p.f.u) and oxides in wt%). (FeO*=FeO+MnO).

(I-type) granites, and Fe-rich in alkaline (A-type) granites. In andesites, biotite is distinguished by an exceptionally high Fe content (FeO=20.81 wt%-26.28 wt%), reflecting characteristics typical of A-type granites. In contrast, biotite in rhyodacites shows lower Fe content (FeO=19.6 wt%-21.87 wt%) and higher Mg content (MgO=10.13 wt%-12.25 wt%), similar to amphibole compositions, which indicates comparable crystallization conditions.

DISCUSSION

General remarks

Amphibole, biotite, pyroxene, and plagioclase are valuable indicators for estimating crystallization conditions, including temperature, pressure, and oxidation states, particularly in calcic amphiboles with elevated calcium content (e.g., Ridolfi et al., 2010, Molina et al., 2015). In this study, both rock types contain calcic amphiboles (Figure 5 b,c) that are euhedral and that exhibit normal zoning indicating a magmatic origin. The absence of reverse and oscillatory zoning in these amphiboles can be considered as evidence of limited fractionation of the parental magma during ascent (Pe-Piper and Piper, 2007). Therefore, the focus of this study is on the quantitative analysis of amphiboles, combined with biotite data from rhyodacitic samples, to infer the geothermobarometric characteristics and magmatic evolution of these rocks.

Amphibole thermobarometric and oxygen fugacity estimate

Pressure estimations derived from Al content in amphiboles provide a reliable geobarometer for determining magma emplacement depth (e.g., Vyhnal et al., 1991; Holland and Blundy, 1994; Ridolfi et al., 2010). The P-T conditions and oxygen fugacity (fO_2) for the alkaline and calc-alkaline rocks (800-1,130 °C, 130– 200 MPa) were estimated with minimal uncertainty (T±23.5 °C, P±11.5%) based on the final experimental database of Ridolfi and Renzulli (2012), which includes 61 amphiboles synthesized in these ranges. For the Kashan andesitic rocks, calculations for Mg-hastingsite and tschermakite indicate that amphiboles crystallized at temperatures of 917-986 °C, most frequently around 950 °C, under lithostatic pressures of 620-800 MPa, peaking at 650 MPa (Figure 7 a,c,d). Similarly, Mg-hornblendes in rhyodacitic rocks crystallized at 780-850 °C, with most frequently around 800 °C, at pressures of 250-450 MPa (Figure 7 a,c,d). Combined, these data suggest a maximum pressure of approximately 650 MPa at 986 °C for andesitic rocks and 400 MPa at 850 °C for rhyodacites, corresponding to crystallization depth of ~28 km and ~16 km respectively, based on the pressure-depth relationship (Putirka et al., 2003).

The magnesium content in amphiboles acts as a key indicator for estimating both the relative fO_2 and NNO (nickel–nickel oxide buffer) and provides insights into the overall oxygen fugacity of calc-alkaline magmas (Ridolfi et al., 2008, 2010). For two types of rocks in this study, the relative fO_2 derived the amphiboles composition, generally ranges from high-temperature magnesiohastingsite (~986 °C and NNO+1.36) to lower-temperature Mg-hornblende (~780 °C and NNO+1.0) (Figure 7b, Table 2). This range aligns with the typical oxygen fugacity range for calc-alkaline magmas, with fO_2 values ranging from NNO -1 to NNO +3 (Ridolfi et al., 2010). Using temperature and pressure estimates from amphibole thermobarometry (Ridolfi et al., 2010), the Kashan andesites and rhyodacitic rocks crystallized under oxygen fugacities of $10^{-9.0}$ bar to $10^{-10.5}$ bar, and $10^{-11.7}$ bar to $10^{-12.8}$ bar, respectively (Table 2).

Hornblende-plagioclase thermometry

Blundy and Holland (1990) developed three calibrations for the amphibole-plagioclase thermometer, focusing specifically on the equilibria of calcic amphibole due to its common coexistence of these minerals in calc-alkaline magmatic rocks. They initially proposed an empirical thermometer based on the edenite-tremolite reaction for temperatures ranging from 500 °C to 1100 °C (Blundy and Holland, 1990). Due to high-temperature estimates in some lithologies, Holland and Blundy (1994) recalibrated the amphibole-plagioclase thermometer, introducing two geothermometers: one for quartz-bearing igneous rocks based on the edenite-tremolite reaction and another for both quartz-bearing and quartz-free igneous rocks based on the edenite-richterite reaction.

Despite continued discussions regarding its accuracy, the amphibole-plagioclase thermometer remains the most applicable geothermometer for calc-alkaline igneous rocks (Stein and Dietl, 2001). Anderson (1996) evaluated various thermometers for hornblende in magmatic rocks and the edenite-richterite thermometer proposed by Holland and Blundy (1994), which provides the most reliable temperature estimates. Nevertheless, in this study, we used the edenite-tremolite thermometer to determine the crystallization temperature of the adakitic andesite and rhyodacitic rocks. This thermometer is specifically calibrated for calc-alkaline magmas, where amphibole-plagioclase equilibria are well-constrained. It also avoids potential overestimation issues associated with the edenite-richterite thermometer in hydrous, mid-crustal systems, which aligns with our inferred crystallization depths. Our preliminary tests showed that the edenite-tremolite thermometer yielded more consistent results with petrographic evidence (e.g., lack of breakdown textures) compared to other calibrations. The results presented in Table 2 (line 5) are for comparison with other calibrations. The calculated temperatures for the

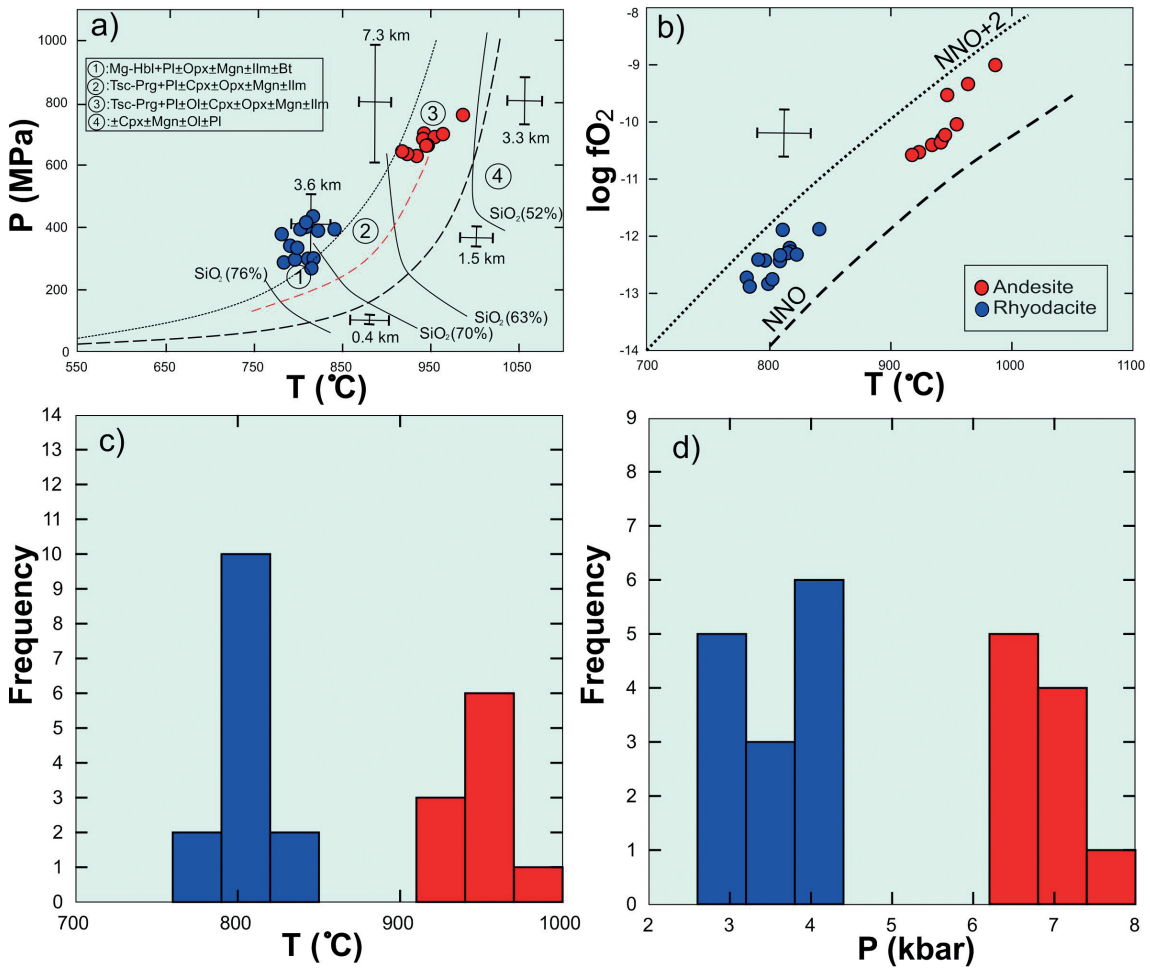

Figure 7. a) P-T (Pressure-Temperature) diagram and, b) log fO_2 versus Temperature diagram (Ridolfi et al., 2010) for the amphiboles from the Kashan adakites; c) and d) Frequency histograms of the temperature and, d) Pressure of crystallization of amphibole in andesitic (red bars) and rhyodacitic (blue bars) rocks.

andesites range from 791 °C to 836 °C (mean=808± 12 °C at 95% confidence), whereas those for the rhyodacitic rocks range from 636 °C to 797 °C (mean=763±33 °C at 95% confidence).

Féménias et al. (2006) developed a quantitative thermometer for high-temperature (>700 °C) amphibole crystallization in Ti-saturated calc-alkaline magma, specifically for magmatic rocks exceeding 800 °C. This thermometer is empirically calibrated to quantify the relationship between Ti content in calcic amphiboles and crystallization temperature, drawing on experimental data from Helz (1979) and Ernst and Liu (1998). The proposed equation is:

Ln[Ti]Amphibole=2603/T-1.70

Using this thermometer, the estimated crystallization temperatures for andesites range from 753 °C to 832 °C (mean=798±28 °C) and for rhyodacitic rocks range from 656 °C to 745 °C (mean=706±35 °C), respectively (Table 2, line 7). These temperature estimates closely match those derived from the Blundy and Holland (1990) amphibole-plagioclase thermometer, further supporting the reliability of this method. This method is best suited for high-Ti amphiboles that crystallized under Ti-saturated conditions, where amphibole coexists with ilmenite, rutile, or titanite. However, its applicability may be limited in systems where Fe-Ti oxides regulate Ti availability or where amphiboles have undergone secondary alteration. While generally considered pressure-independent, high-pressure conditions could affect Ti partitioning, introducing minor uncertainties in temperature estimates. Since the studied samples exhibit mineralogical and geochemical characteristics consistent with these conditions, this thermometer provides a reliable estimate of crystallization temperatures in the Kashan rocks.

Table 2. Calculated thermobarometric results for amphiboles in the Kashan rocks.

Parameter	Andesite									Rhyodacite		
	93J9.11	93J9.12	93J9.13	93J9.14	93J9.15	93J9.16	Gh.28.45	Gh.28.47	Gh.28.44	Jv.an.68	Jv.an.69	Jv.an.70
T (°C)	934.0	942.4	923.3	917.5	941.3	986.3	946.5	944.8	963.7	816.4	826.7	780.9
P(Mpa)	308.7	391.8	322.2	328.2	373.8	468.5	344.0	349.5	386.2	144.1	114.2	111.2
ΔNNO	0.855	0.786	0.903	0.950	0.753	1.360	1.509	0.836	1.408	1.292	1.571	1.010
logfO_2	-10.40	-10.30	-10.52	-10.57	-10.35	-9.00	-9.52	-10.22	-9.33	-12.20	-11.73	-12.72
T1	824.3	817.2	810.8	805.1	805.4	791.3	791.2	836.9	815.2	802.8	782.1	784.5
P1(kbar)	3.0	3.8	3.5	3.7	4.1	5.1	4.3	2.9	3.9	1.6	1.4	1.3
T2	829.5	764.3	760.6	753.0	773.3	781.6	815.3	807.7	793.8	699.0	684.8	656.5
H_2Omelt (wt%)	5.879	6.749	6.581	6.628	6.686	6.205	5.602	5.513	5.618	6.141	5.699	5.756
Continental depth (km)	11.6	14.7	12.1	12.3	14.1	17.6	12.9	13.2	14.5	5.4	4.3	4.2

Parameter	Rhyodacite									
	93k19.90	93k19.91	93k19.92	93k19.95	93k19.97	93k19.98	.93k19.103	cho.84	cho.56	cho.57
T (°C)	783.3	808.3	796.0	790.4	814.6	798.6	833.5	822.2	840.9	808.6
P(Mpa)	115.0	131.7	123.1	104.4	152.3	148.0	150.0	161.2	168.6	111.5
ΔNNO	1.052	1.234	1.509	1.651	1.236	1.035	0.702	1.331	1.119	1.339
logfO2	-12.88	-12.43	-12.42	-12.41	-12.29	-12.83	-12.44	-12.32	-11.87	-12.33
T1	630.2	770.3	797.6	636.3	683.5	647.6	645.9	0	0	0
P1(kbar)	3.1	2.0	1.3	2.9	3.8	4.1	4.1	0	0	0
T2	710.9	745.5	680.4	701.3	671.5	689.1	693.9	0	0	0
H2Omelt (wt%)	5.915	5.653	5.955	5.354	6.561	6.684	6.535	6.544	6.506	5.693
Continental depth (km)	4.3	4.9	4.6	3.9	5.7	5.5	5.6	6.0	6.3	4.2

Note: T(°C)= Temperature calculated using amphibole geothemometer; P (MPa)= Confining pressure on the basis Al-in-amphibole [P=19.209·e(1.438·Altot), from Ridolfi et al., 2010]; NNO= relative oxygen fugacity [NNO= 1.644·(Mg+Si/47-[6]Al/91.3·[6]Ti+Fe^{3+}/3.7+Fe^{2+}/5.2-BCa/20-ANa/2.8+A/9.5), from Ridolfi et al. (2010)]; logfO_2= oxygen fugacity [logfO_2=-.7/(T+273.15)+12.981+(0.046·P·10-1)/(T+273.15)+[-0.5117·ln(T+273.15)]+NNO], from O'Neill and Pownceby (1993); T1 (°C)= temperatures for each P1 (kbar) pressures of hornblende-plagioclase pairs are calculated using plagioclase-hornblende geothermometer by Blundy and Holland (1990); T2= Thermometer amphibole crystallization in Ti-saturated calc-alkaline magma from Féménias et al. (2006); H_2Omelt= Hygrometric equation from Ridolfi et al. (2010); Continental depth (km)= (P/100)·3.7767), from Ridolfi et al. (2010).

Biotite thermometric and oxygen fugacity estimate

Although the Ti concentration in biotite is often used as a geothermometer for metamorphic rocks, where it is closely linked to temperature variations at high temperatures and pressures, recent studies of igneous rocks reveal that the Ti content can be influenced by magmatic processes (e.g., Henry et al., 2005). As demonstrated by Deer et al. (1992), Grant (1986), and Duebendorfer and Frost (1988), the recrystallized biotites in intermediate rocks lose primary thermobarometric signatures. These studies collectively confirm that pervasive recrystallization biotites cannot reliably constrain magmatic conditions. We therefore restricted our thermobarometric analysis to fresh, unaltered amphibole and plagioclase, which better preserve primary crystallization records. The biotites in andesitic samples were excluded from thermobarometric

calculations due their re-equilibrated characteristics.

Biotite Ti levels tend to decrease during magmatic fractionation due to the earlier stages crystallization of Ti-bearing minerals (e.g., Zhang et al., 2016). Henry et al. (2005) suggested a geothermometer for biotite in metapelites based on the Ti content, which has since been to igneous rocks. According to their method, the crystallization temperature of primary biotite in rhyodacitic samples range from 690 to 784 °C (average 712 °C), slightly lower than those of rhyodacitic amphiboles, suggesting biotite crystallized later than amphiboles. Based on the recent geothermobarometric approach proposed by Li and Zhang (2022), the estimated crystallization temperatures closely align with those obtained using the geothermometer of Henry et al. (2005). According to this method, the crystallization temperature of primary biotite in rhyodacitic samples ranges from 750 to 800 °C, with an average of 782 °C, corresponds to a pressure range of approximately 350 to 480 MPa.

Similar to amphiboles, the Fe^{2+}, Fe^{3+}, and Mg contents in biotite can be used to estimate the oxygen fugacity of magmas and associated fluids (Wones and Eugster, 1965). In the ternary Fe^{2+}-Fe^{3+}-Mg diagram (Figure 8a), biotite from rhyodacites is situated close to the NNO buffer line, indicating high oxygen fugacity and formation under oxidizing conditions, consistent with the estimates from amphibole. In the log fO_2-T diagram at P_{H_2O}=207.0 MPa (Figure 8b), the samples plot close to the NNO buffer line and near the hematite-magnetite (HM) buffer, suggesting a relatively high oxidation state during the late stages of biotite crystallization.

Magmatic series and evolution

The chemical composition of amphiboles, in addition to estimating P-T conditions, can also be used to determine the composition of their parent magma and the tectonomagmatic environment (e.g., Molina et al., 2009; Leake, 1971). The compositions of amphiboles from the Kashan adakites are illustrated on Alvi versus KA (Ridolfi and Renzulli, 2012) and SiO_2 versus TiO_2 (Droop, 1987) discrimination diagrams (Figure 9 a,b), confirming their association with the calc-alkaline magma series. Figure 9c illustrates a consistent and positive correlation between Al^{IV} and Al^{total} in the amphiboles, and all values clearly plot within the field of magmatic (igneous) compositions (Hammarstrom and Zen, 1986). Amphiboles in intraplate tectonomagmatic settings have more Na_2O and TiO_2 than those in subduction zone settings (Coltorti et al., 2007); amphiboles from the Kashan adakites are related to a subduction environment (I-amph: Interplate and S-amph: Subduction) (Figure 9d). Additionally, Abdel-Rahman (1994) proposed several magma series and tectonic discrimination diagrams using the FeO, MgO, and Al_2O_3 concentrations in biotites from igneous rocks. According to these diagrams, the biotites from the rhyodacites, which have a magmatic origin, fall within the calc-alkaline field (Figure 10 a,b).

Thermobarometric results indicate that the crystallization depth of magma, as inferred from the mineral chemistry of amphibole, is less than 28 km. In Iran, the Moho depth ranging from approximately 35 km in central Iran to 55 km in the northeastern regions (Motaghi et al., 2012). Taghizadeh-Farahmand et al.

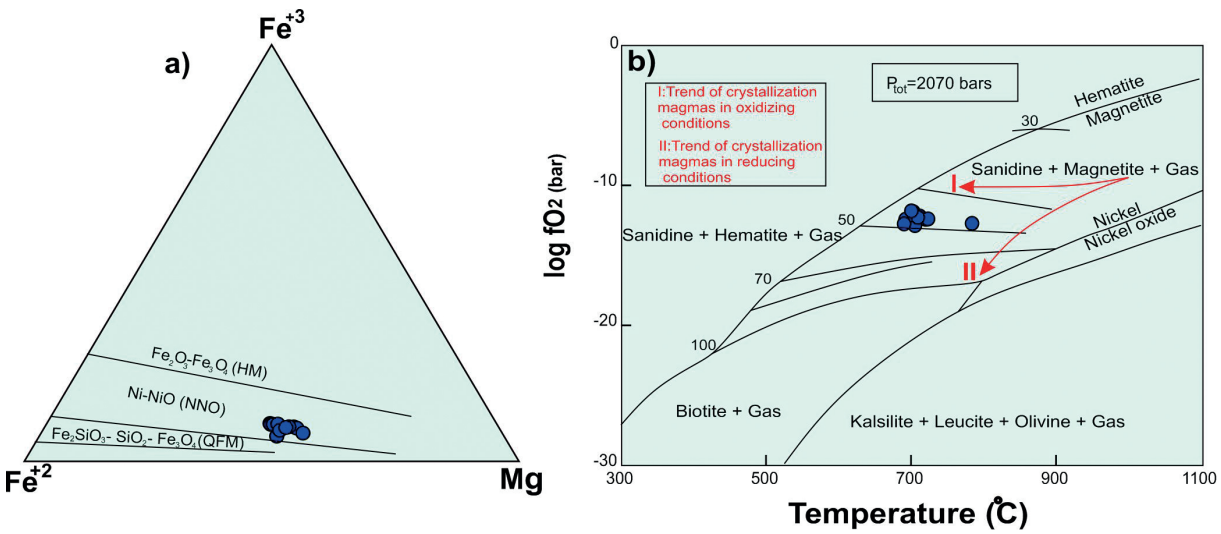

Figure 8. a) Ternary Fe^{2+}- Fe^{3+}- Mg and b) log fO_2- Temperature diagram for biotite+sanidine+magnetite+gas equilibrium at P_{tot}=2070 bars (afterWones and Eugster, 1965). Arrows show trends of crystallization of magmas in oxidizing and reducing conditions (after de Albuquerque, 1973).

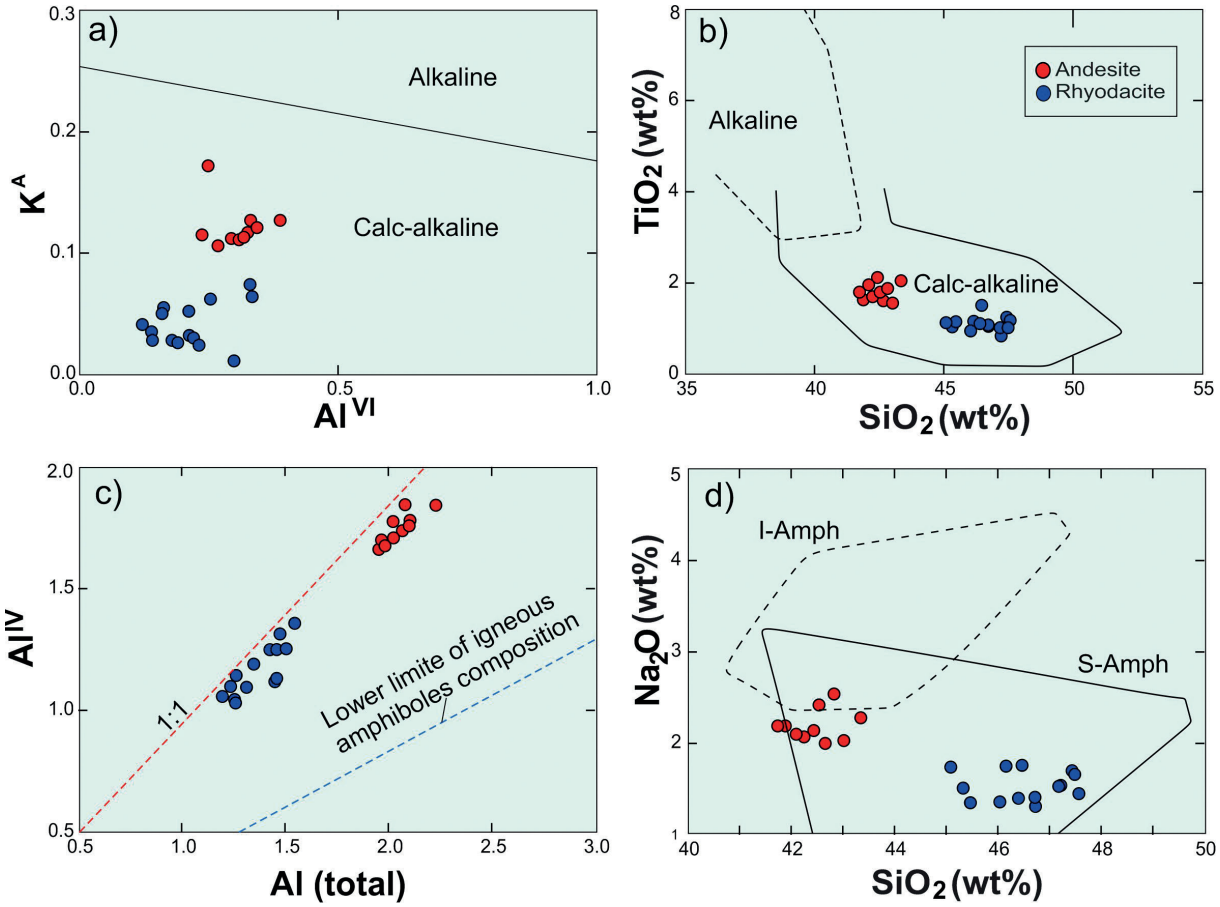

Figure 9. a) Al^{VI} versus K^A diagram (Ridolfi and Renzulli, 2012) and, b) SiO_2 versus TiO_2 discrimination diagram (Droop, 1987) for amphiboles from the Kashan andesitic and rhyodacitic rocks; c) Al total versus Al^{IV} diagram determining amphibole magmatic series (Hammarstrom and Zen, 1986); d) Diagram of Coltorti et al. (2007), indicating that the amphiboles are associated with subduction (I-amph: Interplate and S-amph: Subduction).

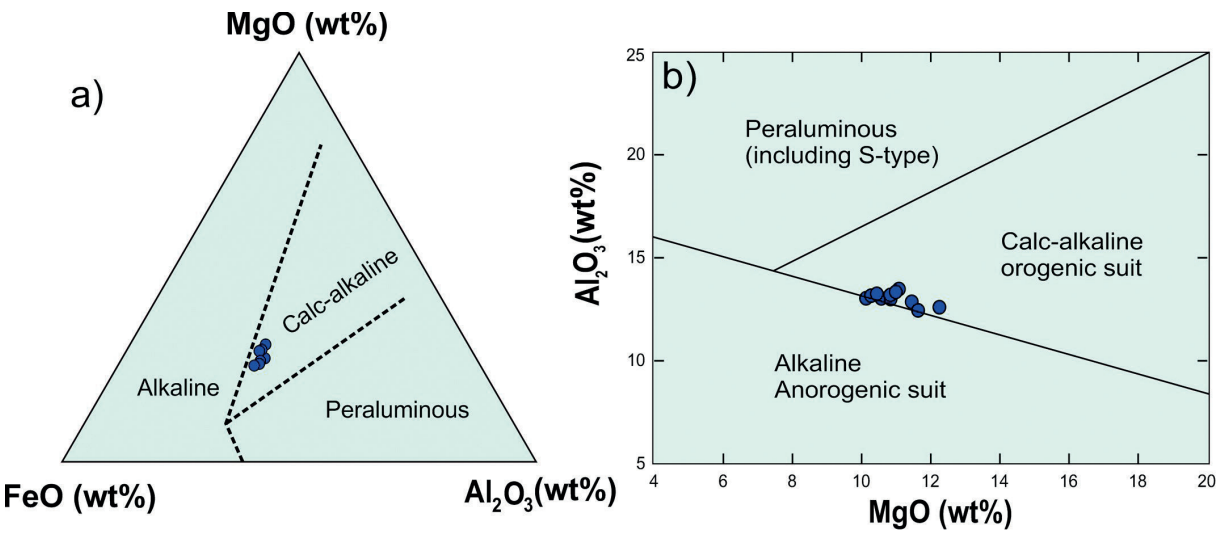

Figure 10. Discrimination diagrams of the biotite in magmatic series from Abdel-Rahman (1994).

(2014) estimated the average Moho depth beneath central Iran to be between 42 and 46 km.

Based on Shafaii Moghadam et al. (2016), the oblique subduction of the Neo-Tethyan oceanic plate beneath Iran is linked to crustal thickening of central UDMA. Omrani et al. (2008) inferred that the Arabia-Eurasia collision began during Oligocene to Early Miocene. They suggested that the Neogene magmatism was linked to the slab-breakoff and consequent thermal re-equilibration in a post-collisional setting. According to Chiu et al. (2013), the majority of Miocene calc-alkaline magmatic activity occurred in the central and southern regions of the UDMA. A shift in the geochemical characteristics from calc-alkaline to adakitic signatures has been identified, coinciding with the collision of the Arabian and Eurasian plates. They suggested that the Middle Miocene adakitic magmatism, attributed to the collision-related crustal thickening, marked the end of arc activities in the Kashan area. Corroborate the findings by Khaksar et al. (unpubl. data), imply that the Kashan Miocene adakitic rocks were probably formed through partial melting of a thickened, mafic lower continental crust, with continuous magmatic underplating providing the necessary heat for melting. Thermobarometric and mineral chemical data from this study confirm that magma crystallization occurred at crustal depths of approximately 28 km for andesites and 16 km for rhyodacites, respectively.

CONCLUSIONS

Comprehensive mineral chemistry and geothermobarometric studies of the Early to Middle Miocene Kashan adakitic rocks (central UDMA), composed of andesite and rhyodacite, provide valuable insights into their formation as is presented in fallowing:

1) The primary minerals identified include amphibole, which ranges from Mg-hastingsite/tschermakite to Mg-hornblende, biotite spanning from annite to phlogopite, and plagioclase that varies from andesine to oligoclase.

2) The crystallization of Mg-hastingsite/tschermakitic amphiboles in andesites occurred at temperatures between 791 and 986 °C, with the most frequent crystallization around 950 °C. These amphiboles formed under lithostatic pressures of 620 to 800 MPa, with the majority of data cluster around 650 MPa. Magnesian-hornblende in the rhyodacites, crystallized at temperatures of 636 to 850 °C, under pressures ranging from 250 MPa to 450 MPa. Additionally, primary biotite in these rocks crystallized at slightly lower temperatures of 690 to 784 °C, with an average of 712 °C.

3) The analysis reveal that magmatic amphiboles exhibit high $Fe^{3+}/(Fe^{3+}+Fe^{2+})$ ratios, whereas biotites from the rhyodacitic rocks are characterized by low total Al contents and narrow Fe/(Fe+Mg) ratios, suggesting relatively oxidizing conditions during the late stages of crystallization. Oxygen fugacity (fO_2) values range from $10^{-10.4}$ bar (ΔNNO+0.75) in andesites to $10^{-12.3}$ bar (ΔNNO+1.7) in rhyodacites, signifying relatively high oxidizing conditions. The crystallization depth of amphiboles during magma evolution in the magma chamber varies from 28 km to 16 km, highlighting the dynamic conditions governing their formation.

ACKNOWLEDGEMENTS

This research originates from the first author's postdoctoral research at Shahrekord University and was funded by the Iran National Science Foundation (INSF; grant number 4013412). This study is partially funded by grants from the Peking University. The authors express their gratitude to Editor Dr. Alessandro Vona for his suggestions and comments, which improved the clarity of this work. Sincere appreciation is also extended to the anonymous reviewers for their insightful comments, which significantly improved the original manuscript.

REFERENCES

Abbott RN. and Clarke DB., 1979. Hypothetical liquidus relationships in the subsystem Al_2O_3–FeO–MgO projected from quartz, alkali feldspar and plagioclase for a (H_2O) 61. Can. Min. J. 17, 549–560.

Abdel-Rahman AM., 1994. Nature of biotites from alkaline, calc-alkaline, and peraluminous magmas. Journal of Petrology 35, 525-541.

Agard P., Omrani J., Jolivet L., Mouthereau F., 2005. Convergence history across Zagros (Iran): Constraints from collisional and earlier deformation. International Journal of Earth Sciences 94, 401-419.

Agard P., Omrani J., Jolivet L., Whitechurch H., Vrielynck B., Spakman W., Wortel R., 2011. Zagros orogeny: A subduction dominated process. Geological Magazine 148, 692-725. doi: 10.1017/S001675681100046X.

Ahmadzadeh G., Jahangiri A., Lentz D., Mojtahedi M., 2010. Petrogenesis of Plio-Quaternary post-collisional ultrapotassic volcanism in NW of Marand, NW Iran. J. Asian Earth Sci. 39, 37-50. doi: 10.1016/j.jseaes.2010.02.008.

Alavi M., 2004. Regional stratigraphy of the Zagros fold-thrust belt of Iran and its proforeland evolution. American Journal of Science 304, 1-20. doi: 10.2475/ajs.304.1.1.

Allen MB., Kheirkhah M., Neill I., Emami M., McLeod CL., 2013. Generation of arc and within-plate chemical signatures in collision zone magmatism: Quaternary lavas from Kurdistan province, Iran. Journal of Petrology 54, 887-911.

Anderson J.F., Barth A.P., Wooden J.L., Mazdab F., 2008. Thermometers and thermobarometers in granitic systems, in Putirka, K.D., Tepley, F.J., III, (Eds.), Minerals, inclusions and volcanic processes. Reviews in Mineralogy and Geochemistry 69, 121-142.

Anderson J.L., 1996. Status of thermobarometry in granitic batholiths. Transactions of Royal Society Edinburgh, Earth

Sciences 87, 125-138.

Azizi H., Nouri F., Asahara Y., Minami M., Whattam S.A., 2024. Continental crust variance between post-collisional compressional and extensional domains controlled magmatic activity at Damavand volcano, Northern Iran. International Geology Review, 1-23. doi: 10.1080/00206814.2024.2370493.

Berberian M. and King G.C.P., 1981. Towards a paleogeography and tectonic evaluation of Iran. Canadian Journal of Earth Sciences 18, 210-265.

Blundy J.D. and Holland T.J.B., 1990. Calcic amphibole equilibria and a new amphibole-plagioclase geothermometer. Contributions to Mineralogy and Petrology 104, 208-224.

Chiu H.Y., Chung S.L., Zarrinkoub M.H., Mohammadi S.S., Khatib M.M., Iizuka Y., 2013. Zircon U-Pb age constraints from Iran on the magmatic evolution related to Neotethyan subduction and Zagros orogeny. Lithos 162-63, 70-87.

Coltorti M., Bonadiman C., Faccini B., Grégoire M.O., Reilly S.Y., Powell W., 2007. Amphiboles from supra-subduction and intraplate lithospheric mantle. J. Aust. Lit. 99, 68-84

Dargahi S., 2007. Post-collisional Miocene magmatism in the Sarcheshmeh Shahrebabak region, NW of Kerman: Isotopic study, petrogenetic analysis and geodynamic pattern of granitoid intrusives and the role of adakitic magmatism in development of copper mineralization. (Unpublished PhD thesis). Shahid Bahonar University of Kerman, pp. 310 (in Persian).

Davoudian A.R., Bendokht M., Shabanian N., Azizi H., Asahara Y., Neubauer F., Genser J., 2022. Geochronology and geochemistry of the Ediacaran orthogneisses from the north Shahrekord (Sadegh-Abad), Sanandaj-Sirjan Zone: Insights into magmatic evolution of the Iranian basement. Geological Journal, 57, 2788-2811.

De Albuquerque, C.A., 1973. Geochemistry of biotites from granitic rocks, northern Portugal. Geochimica et Cosmochimica Acta 37, 1779-1802.

Deer W.A., Howie R.A., Zussman J., 1996. An Introduction to Rock-forming Minerals. 17th Edition, Longman Ltd., London, pp.528.

Delavari M., Amini S., Schmitt A.K., McKeegan K.D., Harrison T.M., 2014. U-Pb geochronology and geochemistry of Bibi-Maryam pluton, eastern Iran: implication for the late stage of the tectonic evolution of the Sistan Ocean. Lithos 200-201, 197-211.

Droop G.T.R., 1987. A general equation for estimating Fe^{3+} concentrations in ferromagnesian silicates and oxides from microprobe analyses, using stoichiometric criteria. Mineralogical Magazine 51, 431-435.

Duebendorfer E.M. and Frost B.R., 1988. Retrogressive dissolution of garnet: Effect on garnet-biotite geothermometry. Geology 16, 875-877.

Ernst W.G. and Liu J., 1998. Experimental phase-equilibrium study of Al-and Ti-contents of calcic amphibole in MORB-A semiquantitative thermobarometer. American mineralogist 83, 952-969.

Fanka A., Tsunogae T., Daorerk V., Tsutsumi Y., Takamura Y., Sutthirat C., 2018. Petrochemistry and zircon U-Pb geochronology of granitic rocks in the Wang Nam Khiao area, Nakhon Ratchasima, Thailand: implications for petrogenesis and tectonic setting. J. Asian Earth Sci. 157, 92-118.

Féménias O., Mercier J.C.C., Nkono C., Diot H., Berza T., Tatu M., Demaiffe D., 2006. Calcic amphibole growth and compositions in calc-alkaline magmas: Evidence from the Motru Dike Swarm (Southern Carpathians, Romania). American Mineralogist 91, 73-81.

Foster M.D., 1960. Interpretation of the composition of trioctahedral micas. United States Geological Survey, Professional Paper 354-B, 1-146.

Ghasemi A. and Talbot C.J., 2006. A new tectonic scenario for the Sanandaj-Sirjan Zone (Iran). Journal of Asian Earth Sciences 26, 683-693.

Ghorbani M.R., Graham I.T., Ghaderi M., 2014. Oligocene-Miocene geodynamic evolution of the central part of Urumieh-Dokhtar Arc of Iran. International Geology Review 56, 1039-1050.

Grant J.A., 1986. The isocon diagram; a simple solution to Gresens' equation for metasomatic alteration. Economic geology 81, 1976-1982.

Hammarstrom J.M. and Zen E.A., 1986. Aluminum in hornblende: an empirical igneous geobarometer. American mineralogist 71, 1297-1313.

Helmy H.M., Ahmed A.F., Mahallawi M.M., Ali S.M., 2004. Pressure, temperature and oxygen fugacity conditions of calc-alkaline granitoids, Eastern Desert of Egypt, and tectonic implications. J. Afr. Earth Sci. 38, 255-268.

Helz R.T., 1987. Differentiation behavior of Kilauea Iki lava lake, Kilauea Volcano, Hawaii: an overview of past and current work. Geochemical Society, Special Publication 1, 241-258.

Henry D.J., Guidotti C.V., Thomson J.A., 2005. The Ti-saturation surface for low to medium pressure metapelitic biotite: Implications for geothermometry and Ti-substitution mechanisms. Am. Mineral. 90, 316-328.

Holland T. and Blundy J., 1994. Non-ideal interactions in calcic amphiboles and their bearing on amphibole-plagioclase thermometry. Contributions to Mineralogy and Petrology 116, 433-447.

Hossain I., Tsunogae T., Rajesh H.M., 2009. Geothermobarometry and fluid inclusions of dioritic rocks in Bangladesh: Implications for emplacement depth and exhumation rate. Journal of Asian Earth Sciences 34, 731-739.

Jahangiri A., 2007. Post-collisional Miocene adakitic volcanism in NW Iran: geochemical and geodynamic implications. J Asian Earth Sci 30, 433-447.

Karsli O., Dokuz A., Uysal I., Aydin F., Kandemir R., Wijbrans R.J., 2010. Generation of the early Cenozoic adakitic volcanism by partial melting of mafic lower crust, Eastern

Turkey: implications for crustal thickening to delamination. Lithos 114, 109-120.

Khaksar T., Rashidnejad-Omran N., Chen F., Song S.G., Li S.Q., Ghaderi M., 2020. Zircon U-Pb ages and magmatic history of the Kashan Plutons in the Central Urumieh-Dokhtar Magmatic Arc, Iran. Evidence for Neotethyan subduction during Paleogene-Neogene: Journal of Earth Science 31, 53-68.

Khaksar T., Rashidnejad-Omran N., Li S.Q., Song S.G., Kananian A., Chen F., Li S., 2022. Geochronology and petrogenesis of granitoids and associated mafic enclaves from Ghohroud in the Urumieh-Dokhtar Magmatic Arc (Iran): Evidence for magma mixing during the closure of the Neotethyan Ocean. Geological Journal, 1-20.

Kheirkhah M., Neill I., Allen M.B., Emami M.H., Ghadimi A.S., 2020. Distinct sources for high-K and adakitic magmatism in SE Iran. J Asian Earth Sci 196, 104355.

Khodami M., Noghreyan M., Davoudian A.R., 2009. Pliocene-Quaternary adakite volcanism in the Isfahan area, Central Iranian magmatic belt. Neues Jahrbuch Fur Mineralogie-Abhandlungen 186, 235-248.

Leake B.E., 1971. On aluminous and edenitic hornblendes. Mineral. Mag. 38, 389-407.

Leake B.E., Woolley A.R., Arps C.E.S., Birch W.D., Gilbert M.C., Grice J.D., Hawthorne F.C., Kato A., Kisch H.J., Krivovichev V.G., Linthout K., Laird J., Mandarino J.A., Maresch W.V., Nickel E.H, Rock N.M.S, Schumacher J.C, Smith D.C, Stephenson N.C.N, Ungaretti L, Whittaker E.J.W., Youzhi G., 1997. Nomenclature of amphiboles: report of the subcommittee on amphiboles of the international mineralogical association, commission on new minerals and mineral names. J. Am. Mineral. 82, 1019-1037.

Li X. and Zhang C., 2022. Machine learning thermobarometry for biotite-bearing magmas. Journal of Geophysical Research: Solid Earth 127, e2022JB024137. doi: 10.1029/2022JB024137

McClusky S., Reilinger R., Mahmoud S., 2003. GPS Constraints on Africa (Nubia) and Arabia Plate Motions Geophysical Journal International 155(1), 126-138. doi: 10.1046/j.1365-246x.2003.02023.x.

Mohajjel M. and Fergusson C., 2000. Dextral transpression in Late Cretaceous continental collision, Sanandaj-Sirjan zone, western Iran. Journal of Structural Geology 22, 1125-1139. doi: 10.1016/ S0191-8141(00)00023-7.

Mohajjel M., Fergusson C., Sahandi M., 2003. Cretaceous-Tertiary convergence and continental collision, Sanandaj-Sirjan Zone, western Iran. Journal of Asian Earth Sciences 21, 397-412. doi: 10. 1016/S1367-9120(02)00035-4.

Molina J., Scarrow J., Montero P.G., Bea F., 2009. High-Ti amphibole as a petrogenetic indicator of magma chemistry: evidence for mildly alkalic-hybrid melts during evolution of Variscan basic-ultrabasic magmatism of central Iberia. Contribution to Mineralogy and Petrology 158, 69-98.

Molina J.F., Moreno J.A., Castro A., Rodriguez C., 2015. Fershtater, G.B. Calcic amphibole thermobarometry in metamorphic and igneous rocks: New calibrations based on plagioclase/amphibole Al-Si partitioning and amphibole/liquid Mg partitioning. Lithos 232, 286-305.

Moradi S., Jiang S.Y., Christiansen E.H., Ghorbani M.R., 2021. Petrogenesis of Tertiary granitoid rocks from east of the Bidhand fault, Urumieh-Dokhtar Magmatic Arc, Iran: Implication for an active continental margin setting. Lithos 400-401, 106422. doi:10.1016/j.lithos.2021.106422.

Motaghi K., Tatar M., Shomali Z.H., Kaviani K., Priestley K., 2012. High resolution image of uppermost mantle beneath NE Iran continental collision zone. J. Phys. Earth Planet. Inter. 208, 38-49.

Nachit H., Ibhi A., Abia E.I.H., Ohoud M., 2005. Discrimination between primary magmatic biotites, reequilibrated biotites and neoformed biotites. Comptes Rendus Geoscience 337, 1415-1420.

Omrani J., Agard P., Whitechurch H., Benoit M., 2008. Arc-magmatism and subduction history beneath the Zagros mountains, Iran: a new report of adakites and geodynamic consequences. Lithos, 106, 380-398.

Pang K.N., Chung S.L., Zarrinkoub M.H., Mohammadi S.S., Yang H.M., Chu C.H., Lee H.Y., Lo C.H., 2012. Age, geochemical characteristics and petrogenesis of Late Cenozoic intraplate alkali basalts in the Lut-Sistan region, eastern Iran. Chemical Geology 306-307, 40-53.

Pang K.N., Chung S.L., Zarrinkoub M.H., Lin Y.C., Lee H.Y., Lo C.H., Khatib M.M., 2013b. Iranian ultrapotassic volcanism at ~11 Ma signifies the initiation of postcollisional magmatism in the Arabia-Eurasia collision zone. Terra Nova 25, 405-413. doi: 10.1111/ter.1205.

Pang K.N., Chung S.L., Zarrinkoub MH., Li X.H., Lee H.Y., Lin T.H., Chiu H.Y., 2016. New age and geochemical constraints on the origin of Quaternary adakite-like lavas in the Arabia-Eurasia collision zone. Lithos 264, 348-359.

Pe-Piper G. and Piper D.J., 2007. Neogene backarc volcanism of the Aegean: New insights into the relationship between magmatism and tectonics.

Putirka K.D., 2008b. Thermometers and barometers for volcanic systems. In: Putrika, K., Tepley, F. (Eds.), Minerals, inclusions and volcanic processes. Rev. J. Mineral. Geochem. 69, 61-120.

Putirka K.D., Mikaelian H., Ryerson F., Shaw H., 2003. New clinopyroxene-liquid thermobarometers for mafic, evolved, and volatile-bearing lava compositions, with applications to lavas from Tibet and the Snake River Plain, Idaho. J. Am. Mineral. 88, 1542-1554.

Radfar J., 1993. Explanatory text of Kashan. Geological quadrangle map 1:100000. No. 6257: Geological Survey of Iran (in Persian).

Ridolfi F. and Renzulli A., 2012. Calcic amphiboles in calc-alkaline and alkaline magmas: thermobarometric and chemometric empirical equations valid up to 1130 °C and 2.2

GPa. Contrib. J. Mineral. Petrol. 163, 877-895.

Ridolfi F., Puerini M., Renzulli A., Menna M., Toulkeridis T., 2008. The magmatic feeding system of El Reventador volcano (Sub-Andean zone, Ecuador) constrained by texture, mineralogy and thermobarometry of the 2002 erupted products. Journal of Volcanology and Geothermal Research 176, 94-106.

Ridolfi F., Renzulli A., Puerini M., 2010. Stability and chemical equilibrium of amphibole in calc-alkaline magmas: An overview, new thermobarometric formulations and application to subduction-related volcanoes. Contributions to Mineralogy and Petrology 160, 45-66.

Rutter M.J., Van der Laan S.R., Wyllie P.J., 1989. Experimental data for a proposed empirical igneous geobarometer: aluminum in hornblende at 10 kbar pressure. Geology 17, 897-900.

Shabanian N. and Neubauer F., 2024. From Early Jurassic intracontinental subduction to Early-Middle Jurassic slab break-off magmatism during the Cimmerian orogeny in the Sanandaj-Sirjan Zone, Iran. Journal of Asian Earth Sciences, 106153.

Shafaii Moghadam H., Li X.H., Stern R.J., Ghorbani G., Bakhshizad F., 2016. Zircon U- Pb ages and Hf-O isotopic composition of migmatites from the Zanjan-Takab complex, NW Iran: Constraints on partial melting of metasediments. Lithos, 240-243, 3448. doi: 10.1016/j.lithos.2015.11.004.

Song S.G., Niu Y.L., Wei C.J., Ji J.Q., Su L., 2010. Metamorphism, anatexis, zircon ages and tectonic evolution of the Gongshan block in the northern Indochina continent An eastern extension of the Lhasa Block. Lithos 120, 327-346.

Song S.G., Niu Y.L., Su L., Wei C.J., Zhang L.F., 2014. Adakitic (tonalitic- trondhjemitic) magmas resulting from eclogite decompression and dehydration melting during exhumation in response to continental collision. Geochimica Et Cosmochimica Acta 130, 42-62. doi.org/10.1016/j.gca.2014.01.008.

Sorensen S.S. and Grossman J.N., 1989. Enrichment of trace elements in garnet amphibolites from a paleo-subduction zone: Catalina schist, southern California. Geochimica et Cosmochimica Acta 53, 3155-3177.

Stein E. and Dietl C., 2001. Hornblende thermobarometry of granitoids from the Central Odenwald (Germany) and their implications for the geotectonic development of the Odenwald. Mineralogy and Petrology 72, 185-207.

Stocklin J., 1968. Structural history and tectonics of Iran: A review. American Association of Petroleum Geology Bulletin 52, 1229-1258.

Szymanowski D., Wotzlaw J.F., Ellis B.S., Bachmann O., Guillong M., Quadt A., 2017. Protracted near-solidus storage and pre-eruptive rejuvenation of large magma reservoirs. Nat. Geosci. 10, 777-782.

Taghizadeh-Farahmand F., Afsari N., Sodoudi F., 2014. Crustal thickness of Iran from converted waves. J. Pure. Appl. Geophys. 172, 309-331.

Torabi G., 2012. Late Permian post-ophiolitic trondhjemites from Central Iran: a mark of subduction role in growth of Paleozoic continental crust. Island Arc 21, 215-229.

Vyhnal C.R., Mcsween H.Y., Speer J.A., 1991. Hornblende chemistry in southern Appalachian granitoids: implications for aluminum hornblende thermobarometry and magmatic epidote stability. J. Am. Mineral. 76, 176-188.

Whitney D.L. and Evans B.W., 2010. Abbreviations for Names of Rock-Forming Minerals. American Mineralogist 95, 185-187. doi: 10.2138/am.2010.3371.

Wones D.R. and Eugster H.P., 1965. Stability of biotite: Experiment, theory, and application. American Mineralogist 50, 1228-1272.

Xiong X.L., Li X.H., Xu J.F., Li W.X., Zhao Z.H., Wang Q., 2003. Extremely high-Na adakite-like magmas derived from alkali-rich basaltic underplate: the late Cretaceous Zhantang andesites in the Huichang Basin, SE China. Geochemical Journal 37, 233-252.

Zhang X., Zhao G., Sun M., Eizenhöfer P.R., Han Y., Hou W., Xu B., 2016. Tectonic evolution from subduction to arc-continent collision of the Junggar ocean: Constraints from U-Pb dating and Hf isotopes of detrital zircons from the North Tianshan belt, NW China. Bulletin, 128, 644-660.